Cranial Parametrization of the Fetal Head for 3D Ultrasound Image Analysis

Ana I. L. Namburete
ana.namburete@eng.ox.ac.uk
Richard V. Stebbing
richard.stebbing@eng.ox.ac.uk
J. Alison Noble
alison.noble@eng.ox.ac.uk

Institute of Biomedical Engineering
Department of Engineering Science
University of Oxford
Oxford, UK

Abstract

We propose a semi-automatic framework for fitting a continuous, parametric surface to cranial boundaries in 3D fetal ultrasound (US) images. The user provides an initial alignment of the surface so that it respects anatomical brain regions. The surface is then deformed to adhere to the cranial boundary, respecting its non-ellipsoidal shape while maintaining the user-provided anatomical alignment. Our framework has applications in preprocessing images for 3D fetal brain image analysis, and for the extraction of clinically useful cranial measurements. We evaluated our framework on 45 fetal US images. An average user time of 1.44 minutes was required for initialization and a visual inspection of results is presented.

1 Introduction

The goal of brain image analysis is to investigate intracranial structures using image information from different subjects and different time points. To achieve this, it is necessary to establish a common coordinate frame between test images. The typical approach for neuroimage preprocessing involves skull stripping followed by registration, in order to deform the images into a common image domain. This inherently relies on the anatomical delineation of internal brain structures within the images.

In developing brains, registration is complicated by absent, underdeveloped, or inconsistent anatomical landmarks for alignment [5]. In particular, analysis of ultrasound (US) images is further complicated by the thickening of cranial bones which results in the obstruction of the intracranial landmarks necessary for registration. However, the skull is reliably visualized due to its echo-bright appearance in comparison to its surrounding tissues. This property of fetal brain US images potentiates the need for a method of obtaining image alignment on the basis of a "cranial domain" as opposed to a "voxel domain". To achieve this, we propose a semi-automatic framework to fit a continuous parametric skull surface into each test image. The domain of the surface acts as the cranial domain, allowing image information to be anatomically queried from any subject based on skull position.

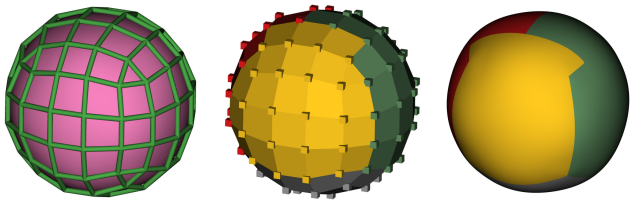

(a) (b) (c)

Figure 1: **Surface Model** (a) The control mesh (green) defines its underlying surface (pink). (b) The control vertices and faces are color-annotated with the anatomical regions with which they will align, and (c) these annotations are propagated down to the surface.

In our framework, the user provides a rough alignment of the skull surface to the imaged brain (Sections 2 and 3). The surface is then minimally deformed to the inner skull boundaries without changing the topology of the surface points (Sections 4 and 5). A discussion of the framework follows in Section 6.

2 Surface Model

A biquadratic B-spline surface specified by control vertices $X \in \mathbb{R}^{N_X \times 3}$ and control mesh $\mathscr{T}$ models the skull surface. A point $\mathbf{p}$ on the surface is parametrized by $\mathbf{u} \in \Omega$, where $\Omega \subset \mathbb{R}^2$, so that $\mathbf{p} = M(\mathbf{u}, X)$ with $M\colon \Omega \times \mathbb{R}^{N_X \times 3} \to \mathbb{R}^3$. The surface normal at $\mathbf{u}$ is defined by $\mathbf{n} = M_\phi(\mathbf{u}, X)$ with $M_\phi\colon \Omega \times \mathbb{R}^{N_X \times 3} \to \mathbb{R}^3$. Exact analytic evaluation of $M(\mathbf{u}, X)$ and $M_\phi(\mathbf{u}, X)$ for *any* control mesh is achieved using Doo-Sabin subdivision [2].

The skull control mesh was crafted to be approximately spherical with 96 vertices and 98 faces (Figure 1(a)). To facilitate the manual initialization process, the vertices and faces of the control mesh were color-annotated with four anatomical landmarks discernible in fetal brain US images: right hemisphere (red), left hemisphere (green), frontal cortex (yellow), falx cerebri (junction between red and green), and base of the brain (gray) (Figure 1(b)). The annotations associated with each point on the control mesh then define the coloring of the underlying surface (Figure 1(c)).

3 Surface Initialization

To initialize the surface control vertices (X^0) the user rigidly aligns the default skull surface to the imaged brain using a multi-view graphical user interface (GUI). This is achieved by manually:

(a) Displacing the center point of the default surface (Figure 2(a)) to roughly align with the center of the brain, and

(b) Rotating and anisotropically scaling the surface such that the surface annotations are roughly aligned to their anatomical positions, approximating the cranial dimensions (Figure 2(b)).

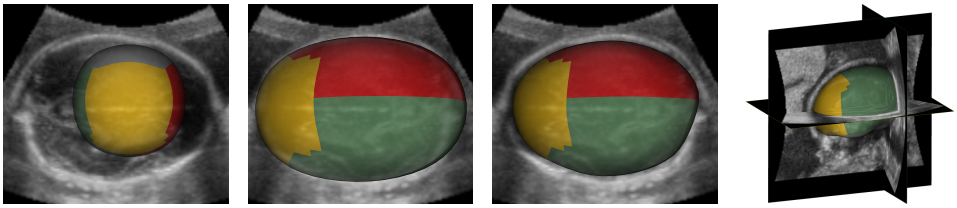

(a) (b) (c) (d)

Figure 2: **Surface Deformation** Axial view of an example fetal head with (a) default annotated surface, (b) user-initialized surface, (c) deformed surface. (d) 3D rendering of deformed cranial surface.

4 Surface Deformation

For a given test image, candidate interior skull positions $C \in \mathbb{R}^{N_C \times 3}$ and normals $\Phi \in \mathbb{R}^{N_C \times 3}$ are generated using standard US edge detection techniques — Feature Asymmetry [4] with an isotropic log-Gabor filter followed by non-maximum suppression.

Given a matrix U of N_U surface points, the energy defining the fit of the surface to some selection $\mathbf{l} \in \mathbb{N}^{N_U}$ of boundary candidates is given by [1]:

$$E(\mathbf{l},U,X) = \sum_{i=1}^{N_U} \underbrace{\left\{ \left\| \mathbf{c}_{l_i} - M(\mathbf{u}_i,X) \right\|^2 + \lambda_1 \left\| \phi_{l_i} - M_\phi(\mathbf{u}_i,X) \right\|^2 \right\}}_{E_{\text{unary}}(l,\mathbf{u},X)} + \underbrace{\lambda_2 \sum_{(i,j)\in\mathcal{N}} \left\| \mathbf{c}_{l_i} - \mathbf{c}_{l_j} \right\|^2}_{E_{\text{pairwise}}(\mathbf{l})}$$

$$+ \underbrace{\lambda_3 \sum_{i=1}^{N_X} \left\| \mathbf{x}_i - \mathbf{x}_i^0 \right\|^2}_{E_{\text{user}}(X)} + \underbrace{\lambda_4 \sum_{(i,j)\in\mathcal{T}} \left\| \mathbf{x}_i - \mathbf{x}_j \right\|^2}_{E_{\text{reg}}(X)} \tag{1}$$

where $\mathcal{N}$ is the set of edges over the surface points and is derived from the Doo-Sabin subdivision procedure and $\Lambda = (\lambda_1,\lambda_2,\lambda_3,\lambda_4)$ controls the influence of each term.

Stepping through Equation 1, E_{unary} quantifies the position and orientation mismatch between each surface point $\mathbf{u}_i$ and its corresponding boundary point l_i. E_{pairwise} models the fact that boundary points are spatially correlated so that neighboring surface points prefer boundary points which are close. E_{user} encourages minimum deformation from the user initialization but more importantly removes the problem of finding multiple local minima that may arise from the geometric symmetry of the near-ellipsoidal shape. E_{reg} encourages a smooth surface by penalizing large displacements between the surface control vertices.

To make the model robust to missing boundary information over large sections of the surface, we augment C with "phantom" boundary candidates which are located at each surface point $\mathbf{p}_i = M(\mathbf{u}_i,X)$ and incur a fixed unary penalty ζ if chosen:

$$E^i_{\text{robust-unary}}(l,\mathbf{u},X) = \begin{cases} E_{\text{unary}}(l,\mathbf{u},X) & l_i \le N_C \\ \zeta & l_i = N_C + i \\ 0 & \text{otherwise} \end{cases} \tag{2}$$

This robust unary $E^i_{\text{robust-unary}}$ replaces E_{unary} in Equation 1, and the augmented candidate matrix is used in place of C in $E_{\text{pairwise}}(\mathbf{l})$.

[1] Note that upper case letters denote matrices and lower case bold letters denote row vectors.

We find a local minimum to Equation 1 by performing alternating discrete and continuous optimization steps (Figure 3). Initializing X to X^0 and U to a regular sampling of Ω, we use belief propagation with a subset of edges in E_{pairwise} to solve for an approximate $\mathbf{l}$ which is then refined using `QPBO` [3]. Next, given $\mathbf{l}$, Equation 1 is minimized *jointly* with respect to X and U using the Levenberg-Marquardt algorithm. Note that if robust labels are chosen during the discrete step, E_{pairwise} is also dependent on X and U because of the "phantom" boundary candidates. It should be emphasized that we do *not* fix U or restrict boundary candidates to be perpendicular to the model surface, which is typically done in "Snakes" and Active Contours. In conjunction with E_{reg}, this strongly discourages surface folding and stretching.

5 Experiments and Results

The cranial deformation model framework was applied to 45 randomly-selected 3D US images of the head from healthy fetuses at 22 weeks of gestation. Each image was typically of dimensions $215 \times 230 \times 151$ with a resolution of $0.2 \times 0.2 \times 0.2\text{mm}^3$. An operator[2] initialized a surface mesh into each individual image, spending an average of **1.44 minutes** per image. Solving time took approximately **2-3 minutes**, dominated by the two discrete optimization steps (Figure 3). Identical model parameters of $\Lambda = (8.0, 3.0, 0.25, 1.0)$, $\zeta = 600.0$, and $N_U = 1536$ were empircally selected and used for all test images. Small changes to Λ and ζ did not result in drastically different recovered surfaces.

Cranial Deformation Our framework updates the control mesh geometry so that the underlying surface matches the cranial boundary. This is evidenced by Figure 4 in which the deformed surfaces are displayed on orthogonal image slices for four of the 45 examples, showing the variability of fetal head pose. Each example highlights that the surface is capable of deforming such that it closely adheres to the inner skull boundaries, respecting the skull's non-ellipsoidal shape.

Anatomical Consistency The deformation process modifies the geometry of the control mesh but preserves topology. To demonstrate this, we first specified cutting planes in the cranial domain. Next, using the deformed surfaces in each image we evaluated these cutting planes in image coordinates (Figure 5). It is evident that the same intracranial structures are visible within the different images, with consistent anatomical positioning. The surfaces provide a cranial parametrization which retains anatomical consistency between images, voiding the need for transformation of the images into a common image voxel domain. However, the anatomical positioning is reliant on a correct anatomical alignment provided by the user initialization.

6 Discussion

We have developed a framework to fit a parametric surface into 3D fetal US scans. This relies on the user to provide a prior for each model surface which is then deformed to fit the interior skull boundary. Our method recovers detailed structure of the skull and anatomically consistent skull surfaces. However, fine-grained alignment is still desirable and our results

[2]The operator did not partake in the development of the graphical user interface or the surface deformation framework.

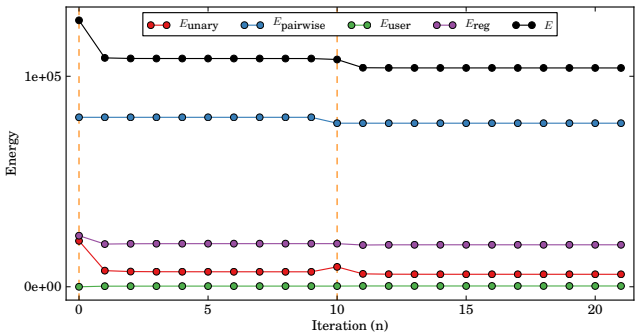

Figure 3: **Example Convergence** ($\zeta = \infty$) Each iteration of discrete optimization ($n = 0, 10$; orange lines) solves for **l**, affecting only E_{unary} and E_{pairwise}. Subsequent continuous optimization steps minimise U and X jointly until convergence, affecting all energies **except** E_{pairwise}. Note the increase in E_{unary} at $n = 10$ is accompanied with a larger decrease in E_{pairwise}.

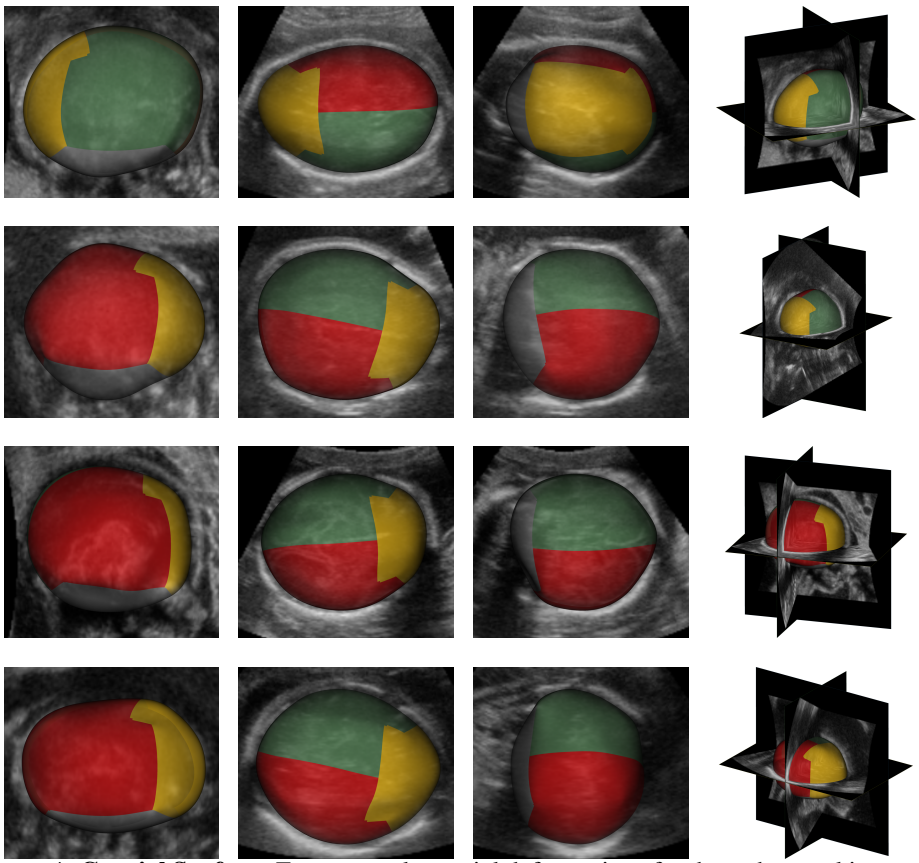

Figure 4: **Cranial Surfaces** Four example cranial deformations for the orthogonal image acquisition slices: coronal (first column), transverse (second column), and axial (third column). The resulting deformed surface (right) is shown for each example.

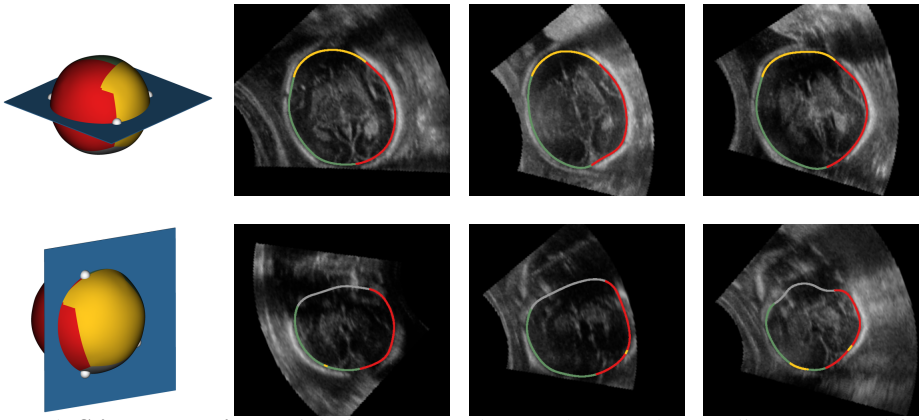

Figure 5: **Slice Extraction** Axial (first row) and coronal (second row) slices extracted from deformed surfaces of six different images at planes defined by 3 points (white). Color annotations display the anatomical consistency between different slices.

show that this should be possible by modeling geometric and appearance similarity between the frames, leading to simultaneous fitting of all model surfaces.

The fact that the surface deforms to adhere to the inner skull boundaries means that it conveniently separates the brain from extracerebral tissue such as the skull, skin, and maternal tissues. Thus, this framework may prove useful as a preprocessing technique for neuroimage analysis algorithms such as segmentation and registration. In addition, the delineation of the cranial outline may allow for the extraction of clinically useful biometric measurements for applications in fetal growth monitoring and detection of craniofacial dysmorphology [1].

References

[1] Hsin-Chen Chen, Pei-Yin Tsai, Hsiao-Han Huang, Hui-Hsuan Shih, Yi-Ying Wang, Chiung-Hsin Chang, and Yung-Nien Sun. Registration-based segmentation of three-dimensional ultrasound images for quantitative measurement of fetal craniofacial structure. *Ultrasound Med Biol*, 38(5):811–823, May 2012.

[2] D. Doo and M. Sabin. Behaviour of recursive division surfaces near extraordinary points. *Computer-Aided Design*, 10(6):356–360, 1978.

[3] V. Kolmogorov and C. Rother. Minimizing nonsubmodular functions with graph cuts-a review. *Pattern Analysis and Machine Intelligence, IEEE Transactions on*, 29(7):1274–1279, 2007.

[4] P. Kovesi. Invariant measures of image features from phase information. *Department of Psychology, University of Western Australia*, 1996.

[5] Colin Studholme. Mapping fetal brain development in utero using magnetic resonance imaging: The big bang of brain mapping. *Annual Review of Biomedical Engineering*, 13(1):345–368, 2011.